

# CKNet: A Convolutional Neural Network Based on Koopman Operator for Modeling Latent Dynamics from Pixels

Yongqian Xiao, Xin Xu, and Lilin Qian,

**Abstract**—For systems with only known pixels, it is difficult to identify its dynamics, especially with a linear operator. In this work, we present a convolutional neural network (CNN) based on the Koopman operator (CKNet) to identify the latent dynamics from raw pixels. CKNet learned an encoder and decoder to play the role of the Koopman eigenfunctions and modes, respectively. The Koopman eigenvalues can be approximated by the eigenvalues of the learned system matrix. We present the deterministic and variational approaches to realize the encoder separately. Because CKNet is trained under the constraints of the Koopman theory, the identified dynamics is linear, controllable and physically-interpretable. Besides, the system matrix and control matrix are trained as trainable tensors. To improve the performance, we propose the auxiliary weight term for multi-step linearity and prediction losses. Experiments select two classic forced dynamical systems with continuous action space, and the results show that identified dynamics with 32-dim can predict validly 120 steps and generate clear images.

**Index Terms**—Koopman Operator, Latent Dynamics, raw pixels, deep learning.

## I. INTRODUCTION

As the identified model is described linearly, model identification with the Koopman operator attracted huge attentions and achieved great successes in recent years. Utilizing the identified model, the controlling performance could be improved via predicting future states and evaluating the corresponding losses. In terms of modeling based on the Koopman operator, two main approaches were proposed in recent years except for deep learning-based methods. One is dynamic mode decomposition (DMD)[1] which applies singular value decomposition (SVD) to extract intrinsic features for approximating the Koopman eigenvalues, eigenfunctions, and modes with the eigenvalues and their corresponding right and left eigenvectors. The other is extended dynamic mode decomposition (EDMD) [2] and its kernel variant K-DMD [3] which transform the modeling into a supervised problem and solves it with least square methods. Koopman operator-based approaches have been applied for approximating the system dynamics in many fields, such as fluid dynamics [4], power system [5], [6], molecular conformation analysis [7], robotic systems [8], etc.

To overcome the dilemma that DMD and EDMD are only applicable to unforced systems, extended methods for forced systems based on DMD and EDMD were designed via dealing

with the state and control input as an augmented matrix [9], [10]. In this way, nonlinear forced systems can be described linearly so that linear control theorems can be applied naturally after planning or for the systems which have explicit reference states [11], [12].

Theoretically, the Koopman operator can accurately describe nonlinear systems globally in the infinite invariant subspace[13], [14]. However, we can not realize infinite-dimensional operator practically. We usually construct a linear operator in a higher-dimensional space to approximate the infinite Koopman operator where the higher-dimensional is created by lifting the original state space via designing basis functions. Basis functions have a decisive effect on modeling performance. They can be constructed with kernel functions, e.g. radial basis functions (RBF), but designing basis functions demands strong experience and lack of theoretical guidance. Besides, when the state's dimension and dataset's scale are extraordinarily large, it is intractable to load all data into memory and execute the SVD or pseudo-inverse operator. In addition, designing proper basis functions is even more complex. DMD, K-DMD, EDMD, and K-EDMD become infeasible.

Deep learning has natural advantages to solve problems of complex function fitting. On basis functions designing problem, we can autonomously train a neural network to take the place of basis functions instead of manually trying different kernel functions with different hyper-parameters. From this perspective, notable researches about combining deep learning and the Koopman operator have fueled its application in many fields such as fluid dynamics[15], power grid[16], vehicle dynamics [17], molecular kinetics[18], atomic scale dynamics[19], highway traffic dynamics [20], chaos system [21] et.al. These works usually adopt an auto-encoder (AE) framework, and the encoder is used to approximate the Koopman eigenfunctions. Besides, some works calculate the system matrix and control matrix according to the sequence of latent states outputted by the encoder[22], [23]. In the meantime, some works treat the system and control matrices as trainable weights [17], [24].

Previous researches mainly focus on low-dimensional systems. However, under many circumstances, existing reasons such as the expensive cost of high-precision sensors, disable us to acquire real-time intrinsic value-wise states, but high-dimensional pixel-wise observations can be grasped via low-cost cameras. Further, pixel-wise observations, such as images or lidar point cloud data, usually include lots of invalid information and noises. In this way, it is intractable to control

the system only according to the inputting raw images. To deal with these situations, learning-based algorithms are usually applied, such as learning-based nonlinear MPC (LB-NMPC) [25], and family of deep reinforcement learning algorithms (DRL) [26], [27]. This end-to-end style leads a poor efficiency, therefore, encoding-based approaches were proposed to learn a neural network model or construct an encoder to improve the learning efficiency, such as MuZero [28], CURL [29], and PlaNet [30]. CURL only extracts features as the state for RL algorithms without predictive ability while MuZero and PlaNet learn a model that takes the extracted feature vector as the latent state with neural networks in an end-to-end style. Unlike with these methods, after features are extracted with the encoder, we regard the feature vector as the latent system's state and adopt the EDMD theory to approximate the Koopman operator of this latent system resulting in an interpretable linear dynamics instead of a non-linear end-to-end model based on neural networks. In this way, we can predict linearly based on the identified dynamics leading to a small computing cost.

Currently, few works focus on approximating the Koopman operator of dynamical systems that take raw pixels as the state. A DMD-based deep learning framework was constructed for background/foreground extraction and video classification [31]. Firstly, it focused on unforced systems. Secondly, it adopts a hierarchical manner that trains AE firstly then does the DMD operator. DeepKoCo [32] is a similar work that the encoder adopts a deterministic approach to output the Koopman eigenfunctions directly. The system matrix consists of Jordan block and the control matrix is subjected to the prediction and reconstruction the next observation. In this work, we adopt EDMD theory with both deterministic and variational approaches that the encoder outputs basis functions which is linear correlation with the Koopman eigenfunctions. The system and control matrices are dealt with trainable tensors. Namely, after training, we obtain the fixed system and control matrices and we can do controllability analysis on the identified latent dynamics.

The main contributions of this work are three-fold:

1) A convolutional neural network based on the Koopman operator is proposed and realized with the deterministic and variational approaches for modeling latent dynamics from raw pixels.

2) An auxiliary weight term is proposed for multi-step linearity and prediction losses to improve the prediction performance. Comparison experiments were designed to study the influence of different auxiliary weights on different losses.

3) The deterministic and variational approaches are applied to identify two classic physical systems with continuous action space. The results show that the proposed method is valid for identifying the latent dynamics from raw pixels and these identified dynamics are controllable.

## II. DESIGN OF CKNET

In this section, we detailedly introduce how to design CKNet for approximating the Koopman operator of discrete-time unforced and forced dynamical systems that taking pixel-wise matrices as states. Also, we give the method for sampling basis functions while we adopt the variational encoder.

### A. CKNet for Unforced Systems

Consider an unforced discrete-time system as follows:

$$x_{k+1} = f(x_k) \quad (1)$$

where  $x \in \mathbb{R}^{c \times h \times w} \in \mathcal{M}$  denotes the state of dynamical system  $f$  in original high-dimension space  $\mathcal{M}$  and it consists of  $c$  images with length  $h$  width  $w$ . We utilize a convolutional neural network (CNN) to approximate the Koopman eigenfunctions, thus the Koopman operator  $\mathcal{K}$  can be defined by

$$(\mathcal{K}\varphi)(x_k) = \varphi(f(x_k)) \quad (2)$$

where  $\varphi \in \mathcal{H}$  are the Koopman eigenfunctions, some space of  $\mathcal{H}$  is usually an infinite-dimensional space. In this manner, the unforced system  $f$  can be described as a linear dynamics in  $\mathcal{H}$ . The linear dynamics evolves linearly in  $\mathcal{H}$ :

$$x_{k+p} = \sum_{i=1} \zeta_i (\mathcal{K}^p \varphi_i)(x_k) = \sum_{i=1} \zeta_i \mu_i^p \varphi_i(x_k) \quad (3)$$

where  $\mathcal{K}^p$  denotes  $p$  times Koopman operator,  $\mu_i$  is the  $i$ -th Koopman eigenvalue corresponding to the  $i$ -th Koopman eigenfunction  $\varphi_i$ , and  $\zeta_i$  is the  $i$ -th Koopman mode to remap states back to  $\mathcal{M}$ .

Though  $\mathcal{K}$  operator is acted in infinite-dimensional space, it attracts attention because of its linearity. Methods of DMDs approximate the Koopman operator via approximating the Koopman eigenvalues, eigenfunctions, and modes. In this work, we propose a deep learning framework based on EDMD to approximate the Koopman operator, unlike DMDs. Because of the limitation of length, no more tautology here. Want more details of EDMD could refer to [2], [11]. As shown in Fig. 1, CKNet expands a low-dimensional subspace  $\mathcal{V}$  via the encoder  $\phi$  to extract intrinsic dynamical features as basis functions to play the role of the Koopman eigenfunctions. Meanwhile, a nonlinear CNN decoder is designed to play the role of the linear Koopman modes to transform latent states from  $\mathcal{V}$  back to pixels in  $\mathcal{H}$ . Therefore, the unforced system  $f$  can be approximated via CKNet:

$$\begin{cases} \phi(x_{k+p}) \doteq \phi_{\mathcal{K}}(x_{k+p}) = \mathcal{K}^p \phi(x_k) = A^p \phi(x_k) \\ x_k = \tilde{\phi}(x_k) \end{cases} \quad (4)$$

where  $\mathcal{K}$  is an approximating operator of  $\mathcal{K}$  in  $\mathcal{V}$  and represented by the square matrix  $A$ ,  $\phi(x) \in \mathbb{R}^L$  and  $\phi_{\mathcal{K}}(x) \in \mathbb{R}^L$  denote the latent state acquired via the encoder and  $\mathcal{K}$  operator, respectively,  $\tilde{\phi}(\phi(x)) \in \mathbb{R}^{c' \times h \times w}$  denotes the output of the decoder, where  $c'$  is a hyper-parameter which equals  $c$  or 1. After training, the Koopman eigenvalues are approximated by the eigenvalues of  $A$ . Note that basis functions is linear correlation with Koopman eigenfunctions. That is,  $\varphi_i = a_i^T \phi(x)$ , where  $a_i$  is the right eigenvector corresponding to the  $i$ -th eigenvalue.

With the deterministic approach, the encoder outputs basis functions  $\phi(x)$  directly. While the encoder adopts the variational approach, we can acquire the basis functions via sampling from the learned Gaussian distribution. To realize back-propagation, reparameterized technique is applied to

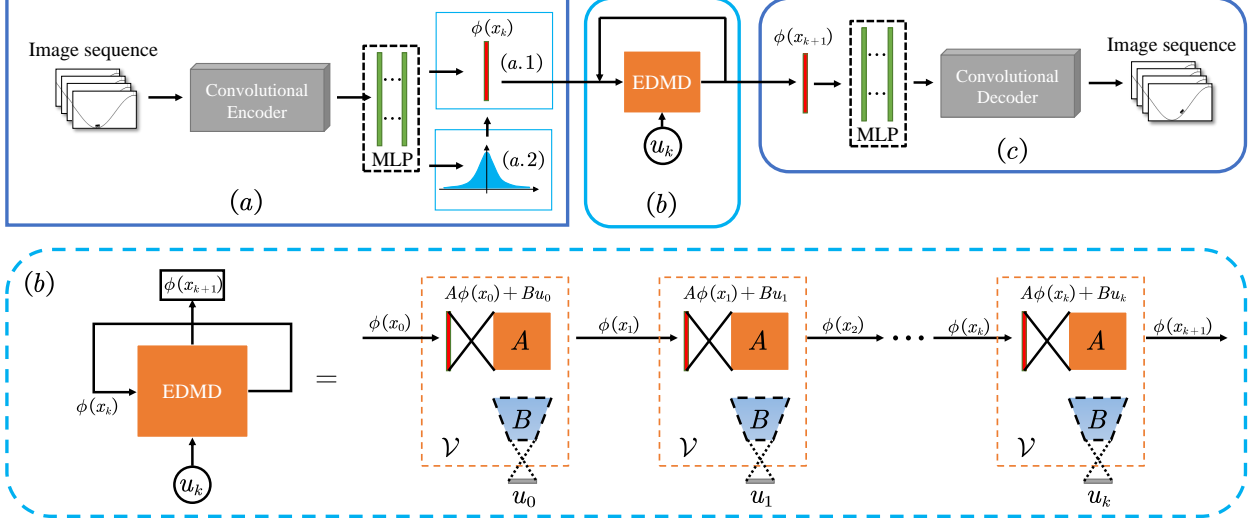


Fig. 1. The framework of CKNet. (a) The encoder of CKNet for expanding some finite space of  $\mathcal{V}$  as an invariant subspace of  $\mathcal{H}$ . It outputs basis functions for taking the place of the Koopman eigenfunctions. We construct the encoder in two ways, the deterministic approach and the variational approach respectively. The deterministic approach shown in (a.1), outputs basis functions directly after the MLP. (a.2) shows the variational approach via sampling from the learned Gaussian distribution. (b) We adopt a recursive way to realize multi-step training. A high-dimensional nonlinear systems can be described as a low-dimensional linear dynamics  $\phi(x_{k+1}) = A\phi(x_k) + Bu_k$  in  $\mathcal{V}$ , where the system matrix  $A$  and control matrix  $B$  are obtained as trainable tensors. CKNet is also applicable for unforced systems while the input  $u_k$  equals 0 constantly. (c) The decoder has the reverse structure with the encoder and it plays the role of the Koopman modes for mapping the latent state from subspace  $\mathcal{V}$  back to the original observation space.

sample basis function in the training process:

$$\phi(x) = \mu_\phi(x) + \exp(\ln(\sigma_\phi(x)) \odot \xi) \quad (5)$$

where  $\mu_\phi$  and  $\sigma_\phi$  are the mean and variance of the learned Gaussian distribution. The  $\mu$  and  $\ln(\sigma_\phi)$  are given by the variational encoder. Where  $\xi \mathcal{N}(0, I)$  is a noise vector from a standard normal distribution.

### B. CKNet for Forced Dynamics

In this section, we focus on approximating forced dynamics with CKNet. Consider a discrete-time forced dynamics:

$$x_{k+1} = f(x_k, u_k) \quad (6)$$

where  $x_k \in \mathbb{R}^{c \times h \times w}$  and  $u_k \in \mathbb{R}^n$  are the state and control of the system  $f$ . There are several methods of extending the Koopman operator for forced systems which take value-wise vector as states[9], [10], [11]. In this work, we adopt the method in [11]. The Koopman operator of (6) can be described as follows:

$$(\mathcal{K}\varphi) \mathcal{X}_k = \varphi(f(\mathcal{X}_k)) \quad (7)$$

where  $\mathcal{X}$  is the extended state of the dynamics:

$$\mathcal{X}_k = \begin{bmatrix} x_k \\ u_k \end{bmatrix}$$

Similarly, CKNet is also applicable for approximating the Koopman operator in (7):

$$\begin{cases} \phi(x_{k+p}) \doteq \phi_{\mathcal{X}}(x_{k+p}) = \mathcal{G}^p \Psi(x_k) \\ x_k = \tilde{\phi}(x_k) \end{cases} \quad (8)$$

where  $\mathcal{G} = [A \ B]$  is an approximating operator for forced dynamics.  $\Psi(x_k) = [\phi(x_k) \ u_k]^\top$  is the extended state in  $\mathcal{V}$ .

In EDMD, the system matrix  $A$  and control matrix  $B$  are solved by constructing a least square problem that builds the dataset with snapshot pairs. However, it is not feasible for large-scale dynamical systems. In this work, we treat  $A$  and  $B$  as trainable tensors and train them in a mini-batch manner.

Particularly, we execute the controllability analysis of the identified dynamics in subspace  $\mathcal{V}$  in the training process. The approximated discrete-time linear dynamics is controllable if the following matrix  $S$  is full rank:

$$\begin{cases} S = [B \ AB \ A^2B \ \dots \ A^{L-1}B] \\ \mathcal{R} = \text{Rank}(S) \end{cases} \quad (9)$$

### C. Loss functions for CKNet

CKNet is a general framework based on the classic EDMD theory. Meanwhile, CKNet extends the scope of application mainly in three aspects: Firstly, CKNet adopts multi-step loss functions to improve the approximating performance while EDMD adopt one-step loss functions. Secondly, CKNet is applicable for pixel-wise inputted dynamical systems while EDMD is only applicable for value-wise systems. Thirdly, CKNet adopts a mini-batch training manner, but EDMD trained via solving a least square problem with whole training data so that EDMD is not feasible for high-dimensional systems.

To strength the linear accuracy of the identified model in  $\mathcal{V}$ , we consider the term of linearity loss to restrain the encoder. Multi-step linearity loss technology is applied so that the approximated dynamics can be identified better in a global

perspective leading to more predictive steps without divergence.

$$\begin{aligned} L_{linear} &= \frac{1}{p_l} \sum_{i=1}^{p_l} \varrho_i \|\phi(x_{k+i}, \theta_e) - \phi_{\mathcal{K}}(x_{k+i})\|_F^2 \\ &= \frac{1}{p_l} \sum_{i=1}^{p_l} \varrho_i \|\phi(x_{k+i}, \theta_e) - \mathcal{G}^i \Psi(x_k)\|_F^2 \end{aligned} \quad (10)$$

where the encoder  $\phi$  is parameterized with trainable weights  $\theta_e$ ,  $\varrho_i$  is the weight of the  $i$ -th step linear prediction,  $\mathcal{G}^i$  denotes  $i$  times linear recursion from a state  $\phi(x_k, \theta_e)$  with a sequence of control  $u_k, \dots, u_{k+i}$  in  $\mathcal{V}$ , and it can be calculated as follows:

$$\begin{aligned} \mathcal{G}^i \Psi(x_0) &= \phi_{\mathcal{K}}(x_{k+i}) \\ &= A \phi_{\mathcal{K}}(x_{k+i-1}) + B u_{k+i-1} \\ &= \dots \\ &= A^i \phi(x_k, \theta_e) + \sum_{j=1}^i A^{j-1} B u_{k+i-j} \end{aligned} \quad (11)$$

When we train the encoder,  $A$ , and  $B$  only with the constraint (10), we can also acquire a linear approximated dynamics in  $\mathcal{V}$  if we don't demand to obtain corresponding pixels. However, during the training process, this training way will make the encoder,  $A$ , and  $B$  converging to zeros gradually which results in an invalid model. To avoid this problem, a reconstruction loss function is included. This loss restrains the intrinsic features extracted by the encoder to contain all the information so that the decoder could retrieve original pixels.

$$L_{recon} = \frac{1}{p} \sum_{i=1}^p \left\| x_k - \tilde{\phi}(\phi(x_{k+1}, \theta_e), \theta_d) \right\|_F^2 \quad (12)$$

where  $\tilde{\phi}$  denotes the decoder which is parameterized with  $\theta_d$ .

Since we need to generate the corresponding images after multi-step prediction in  $\mathcal{V}$ , the weighted multi-step prediction loss function is designed to further restrain the encoder and decoder.

$$L_{pred} = \frac{1}{p_p} \sum_{i=1}^{p_p} \iota_i \left\| x_k - \tilde{\phi}(\mathcal{G}^i \Psi(x_k), \theta_d) \right\|_F^2 \quad (13)$$

where  $\iota_i$  is the weight for the  $i$ -th step linear prediction.

Pixel-wise inputted systems are more complex and tough to approximate than value-wise systems because raw pixels state contain many invalid noises. Leading to a problem that, after some prediction steps generated images only have the background information, but lost all key features. To alleviate this problem, we add a term of auxiliary weight to increase the importance of losses of long step's prediction.  $\varrho_i$  in (10) and  $\iota_i$  have similar functions in this work, and they are defined by a 'tanh' function as follows:

$$\begin{cases} \iota_i = 1 + \tanh(\tau_l i) \\ \varrho_i = 1 + \tanh(\tau_p i) \end{cases} \quad (14)$$

where  $\tau_*$  is a hyper-parameter and it influences the importance degree as shown in Fig. 2. In this way, weights  $\iota$  and  $\varrho$  are limited in the range of [1 2] so that they will not cause gradient explosion.

In addition, we add a term of  $l_2$  regulation loss on the

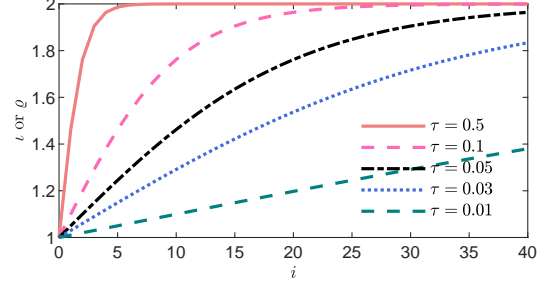


Fig. 2. The weight of multi-step loss functions. We can change the importance degree of the  $i$ -th step prediction loss via tune  $\tau$ . When the total prediction steps  $p_l$  or  $p_p$  in the training process is large, we should tune down the value of  $\tau$ , increase it vice-versa.

encoder and decoder to avoid over-fitting.

$$l_2 = \Theta^2 \quad (15)$$

where  $\Theta$  denotes the weights of the encoder, decoder,  $A$ ,  $B$ .

Finally, CKNet can be trained under the loss function as follows:

$$L = \alpha_1 L_{linear} + \alpha_2 L_{recon} + \alpha_3 L_{pred} + \alpha_4 l_2 \quad (16)$$

where  $\alpha_1, \alpha_2, \alpha_3, \alpha_4$  are the weights for each loss function. We can train CKNet through minimizing the weighted loss,  $L$ , details shown in Algorithm 1.

---

**Algorithm 1** The CKNet Algorithm

---

**Require:**  $p, p_l, p_p, \tau_l, \tau_p, \tau, \tau_*, c, c', \zeta, lr, Epoch = 0, Epoch_{max}, \alpha_i, i = 1, \dots, 4$ , batch size  $b_s$ , a small scalar  $\epsilon > 0$ .  
 Initialize  $\theta_e, \theta_d, A, B$   
**Ensure:** trained  $\theta_e, \theta_d, A, B$ ;

- 1: **while**  $Epoch > Epoch_{max}$  **do**
- 2:     Sample a batch data sequence of images and controls with the length of  $ms = \max(p, p_l, p_p)$ .  $x_{1:ms+c}, U_{1:ms}$
- 3:     **for**  $i = 1$  **to**  $ms$  **do**
- 4:         **if** Adopt deterministic approach **then**
- 5:             Obtain the latent state,  $\phi(x_{i:i+c}, \theta_e)$ , outputted by the encoder directly;
- 6:         **else**
- 7:             Sample the latent state  $\phi(x_{i:i+c}, \theta_e)$  with (5);
- 8:         **end if**
- 9:         Acquire the reconstruction state  $\hat{x} = \tilde{\phi}(\phi(x_{i:i+c}, \theta_e), \theta_d)$ ;
- 10:     **end for**
- 11:     **for**  $i = 1$  **to**  $ms$  **do**
- 12:         Compute  $\mathcal{G}^i \Psi(x_{1:1+c})$  with (11) and  $\tilde{\phi}(\mathcal{G}^i \Psi(x_{1:1+c}))$ ;
- 13:     **end for**
- 14:     Obtain the weighted loss  $L$  in (16) with (10), (12), (13), (14), and (15);
- 15:     Update  $\theta_e, \theta_d, A$ , and  $B$  via minimizing  $L$  with an Adam optimizer;
- 16:      $Epoch = Epoch + 1$
- 17: **end while**

---

TABLE I  
INFORMATION OF COLLECTED DATASET.

	CARTPOLE	MOUNTAINCAR
EPISODES	250	240
STEPS	[200 300]	[300 400]
ALLOCATION	[25 25 200]	[20 20 200]

### III. EXPERIMENTS

In this work, we adopt the offline training manner to validate our CKNet via two nonlinear pixel-wise inputted systems with continuous action space, MountainCar and CartPole, respectively. Namely, we first collect the training, testing, and validation datasets, and preprocess these data before training.

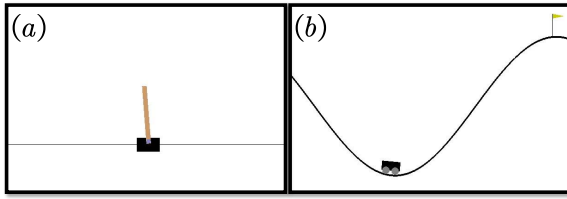


Fig. 3. The selected two forced dynamics in Gym environment with continuous action space for validating CKNet. (a) Modified ‘CartPole-v0’ task with continuous action space; (b) ‘MountainCarContinuous-v0’ task.

#### A. Data collection

‘MountainCarContinuous-v0’ and ‘CartPole-v0’ are two classic tasks for validating reinforcement learning (RL) algorithms. In gym library, the MountainCar task provides the version with continuous action space while CartPole task only supports discrete action space with  $\{-10, 0, 10\}$ . Thus we did a slight modification to support continuous action space for the CartPole task. In order to obtain comprehensive data in the state space, we utilize trained RL algorithms and plus a term of noise to the controller for data collection. In collecting process, we record episodes data including the current image  $s_k$ , the executed control  $u_k$ , and the next image  $s_{k+1}$ . For CartPole, we collected 250 episodes where 25 for testing, 25 for validation, and the rest 200 for training. The steps of each episode are in the range of [200 300]. Similarly for MountainCar, information is detailed in Table. I.

In the preprocessing, we first convert images to grayscale. Then, we enhance these images by modifying the grayscale to 1.0 when a pixel’s value is bigger than 0.8. Lastly, we crop and resize images to an appropriate size so that we can decrease the calculation cost but still keep enough key information..

A single image include position and angle features but it can not represent information of velocities, such as velocity of the car and angular velocity of the pole In the CartPole task. Therefore, we concatenate  $c$  continuous images to a multi-channel tensor as the state. Consequently, the size of state tensors is  $c \times 460 \times 170$  for CartPole environment,  $c \times 90 \times 90$  for MountainCar.

TABLE II  
NEURAL NETWORK STRUCTURE OF THESE TWO EXAMPLES.

CARTPOLE STRUCTURE	ACT	MOUNTAINCAR STRUCTURE	ACT
$170 \times 460 \times 3$	INPUT	$90 \times 90 \times 3$	INPUT
$84 \times 229 \times 8$	RELU	$44 \times 44 \times 16$	RELU
$41 \times 113 \times 16$	RELU	$21 \times 21 \times 32$	RELU
$19 \times 55 \times 32$	RELU	$9 \times 9 \times 64$	RELU
$8 \times 26 \times 64$	RELU	$6 \times 6 \times 128$	RELU
$3 \times 12 \times 128$	RELU	-	-
4860	RELU	4860	RELU
1525	RELU	1525	RELU
32	-/TANH	32	-/TANH

#### B. Training

As shown in Table. II, the neural networks have similar structures and they are designed simply without any pooling layer. There is one more convolutional layer considering that the input image of the CartPole task is bigger. For the activation function of the encoder’s last layer, we tried two kinds of activation styles, ‘Tanh’ function and without an activation function, and simulation results show that these two styles are both valid. Decoders have completely reversed structures with corresponding to encoders. Activation functions of decoders are ‘ReLU’ function except the activation function of the last convolutional layer is ‘Sigmoid’ function.

Hyperparameters are given in Table. III, where  $lr$ ,  $bs$  are the learning rate and batch size respectively,  $c$  and  $c'$  denote the number of images for the input of encoders and output of decoders. When  $c' = c$ , it means the decoder is constrained to output the exact images corresponding to the input of the encoder. When  $c' = 1$ , it denotes the decoder is only constrained to output the current image which equals the last image of the input of the encoder. From Table. III we can know that hyperparameters of these two tasks are almost the same except for the learning rate and batch size. In the training process, CKNet does not need to design network structure and tune hyperparameters deliberately for different tasks.

Additionally, we train the network with Pytorch-Lightning 1.0.7, which is a framework based on Pytorch. Pytorch-Lightning is convenient for training with multi-GPU and synchronizing parameters of batch-normalization. We train these networks with four NVIDIA GeForce GTX 2080Ti GPU with batch-normalization.

### IV. RESULTS

During training process, we regularly check the controllability of the identified linear dynamics via recording the rank of  $S$  in (9). The change curve of the rank  $\mathcal{R}$  shown in Fig. 4, for CartPole task, the rank  $\mathcal{R}$  reaches  $V$  quickly, where  $V$  is the dimension of the latent state. For the MountainCar task,  $S$  becomes full rank after around 4.5K training steps. Namely, in the training process, the identified models of these two tasks for both deterministic and variational approaches become controllable.

TABLE III  
HYPER-PARAMETERS OF TWO ENVIRONMENT.

CARTPOLE		MOUNTAINCAR	
H-PARAM	VALUE	H-PARAM	VALUE
$\alpha_1$	0.3	$\alpha_1$	0.3
$\alpha_2$	1.0	$\alpha_2$	1.0
$\alpha_3$	1.0	$\alpha_3$	1.0
$\alpha_4$	$5 \times 10^{-7}$	$\alpha_4$	$5 \times 10^{-7}$
$V$	32	$V$	32
$\tau_p$	0.03	$\tau_p$	0.03
$\tau_l$	0.03	$\tau_l$	0.03
$p_l$	25	$p_l$	25
$p_p$	25	$p_p$	25
$p$	25	$p$	25
$c$	3	$c$	3
$c'$	3	$c'$	3
$lr$	0.0004	$lr$	0.0001
$bs$	16	$bs$	32

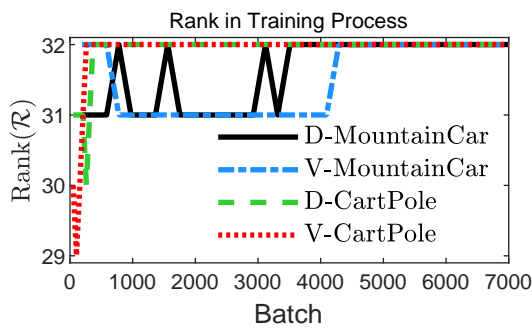


Fig. 4. The rank in the training process of the matrix  $S$  in (9).  $\star$  denotes the realized task  $\star$  with the deterministic approach, and where  $\star \in \{ \text{MountainCar}, \text{CartPole} \}$ .  $V\star$  denotes the variational approach for the task of  $\star$ .

For testing, we do 120 steps prediction of these two tasks for demonstrating the proposed CKNet. We first obtain the original latent state  $\phi(x_0)$  utilizing the original state  $x_0$  which consists of  $c$  adjacent images, then we acquire  $\phi_{\mathcal{K}}(x_{0:k-1})$  with a sequence of controls  $u_{1:k}$  as input according to the recurrent rule as shown in Fig. 1 (b).

Because the dimension of the latent state equals 32 in this work, for intuitive expression, we adopt the mean absolute error (MAE) of each step of the latent state and reconstruction image to evaluate the accuracy of identified linear dynamics. Generally, there are two ways while utilizing the identified dynamics. While we use the latent state as the input of systems for controlling, we expect a smaller error on predicted latent states. Similarly, while we use predicted images, we desire a smaller error on generation images. As shown in Fig. 5, we study the influence of auxiliary weights on the prediction performance with deterministic and variational approaches.

In the MountainCar task, we can knowledge that an appropriate auxiliary weight on linearity loss can significantly decrease the prediction of latent states with both deterministic and variational approaches. For image prediction and generation, an appropriate auxiliary weight also has an obvious improvement when the prediction step is within the range of [0 80] steps for

the deterministic approach, and [0 50] steps for the variational approach.

In the CartPole task, auxiliary weights have obvious performance improvements on prediction of generation images for both deterministic and variational approaches. For latent states prediction, auxiliary weights on  $L_{pred}$  have a better assistance for the deterministic approach while auxiliary weights are putted on  $L_{linear}$ . Besides, small auxiliary weights on  $L_{pred}$  are more suitable.

The prediction and images generation result shown in Fig. 6 and Fig. 7, identified dynamics can not only accurately predict dynamical intrinsic state, such as the position, angle, and velocities, but also contain fixed information of environments, i.e. the size of the pole, the shape and slide rail of the car, the shape of the mountain.

## V. CONCLUSION

This work proposes a deep learning framework with convolutional networks for identifying the latent dynamics from raw images. We construct the encoder in two different ways, the deterministic and variational approaches. Besides, auxiliary weights are introduced into multi-step linearity and prediction losses to improve the prediction performance. Training process under the constraints of the Koopman operator, the identified model is linear, controllable, and physically-interpretable in the subspace constructed by the encoder. Experiments adopt two classic forced and unforced physical systems with continuous action space and the results show that the identified model can accurately predict the latent states and generate clear images for 120 steps linear prediction.

## ACKNOWLEDGMENT

The authors would like to thank...

## REFERENCES

- [1] P. J. Schmid, "Dynamic mode decomposition of numerical and experimental data," *Journal of fluid mechanics*, vol. 656, pp. 5–28, 2010.
- [2] M. O. Williams, I. G. Kevrekidis, and C. W. Rowley, "A data-driven approximation of the koopman operator: Extending dynamic mode decomposition," *Journal of Nonlinear Science*, vol. 25, no. 6, pp. 1307–1346, 2015.
- [3] I. G. Kevrekidis, C. W. Rowley, and M. O. Williams, "A kernel-based method for data-driven koopman spectral analysis," *Journal of Computational Dynamics*, vol. 2, no. 2, pp. 247–265, 2016.
- [4] I. Mezić, "Analysis of fluid flows via spectral properties of the koopman operator," *Annual Review of Fluid Mechanics*, vol. 45, pp. 357–378, 2013.
- [5] Y. Susuki, I. Mezic, F. Raak, and T. Hikihara, "Applied koopman operator theory for power systems technology," *Nonlinear Theory and Its Applications, IEICE*, vol. 7, no. 4, pp. 430–459, 2016.
- [6] M. Netto and L. Mili, "A robust data-driven koopman kalman filter for power systems dynamic state estimation," *IEEE Transactions on Power Systems*, vol. 33, no. 6, pp. 7228–7237, 2018.
- [7] S. Klus, A. Bittracher, I. Schuster, and C. Schütte, "A kernel-based approach to molecular conformation analysis," *The Journal of Chemical Physics*, vol. 149, no. 24, p. 244109, 2018.
- [8] G. Mamakoukas, M. L. Castano, X. Tan, and T. Murphey, "Local koopman operators for data-driven control of robotic systems," in *Robotics: science and systems*, 2019.
- [9] J. L. Proctor, S. L. Brunton, and J. N. Kutz, "Dynamic mode decomposition with control," *SIAM Journal on Applied Dynamical Systems*, vol. 17, no. 1, pp. 142–161, 2018.

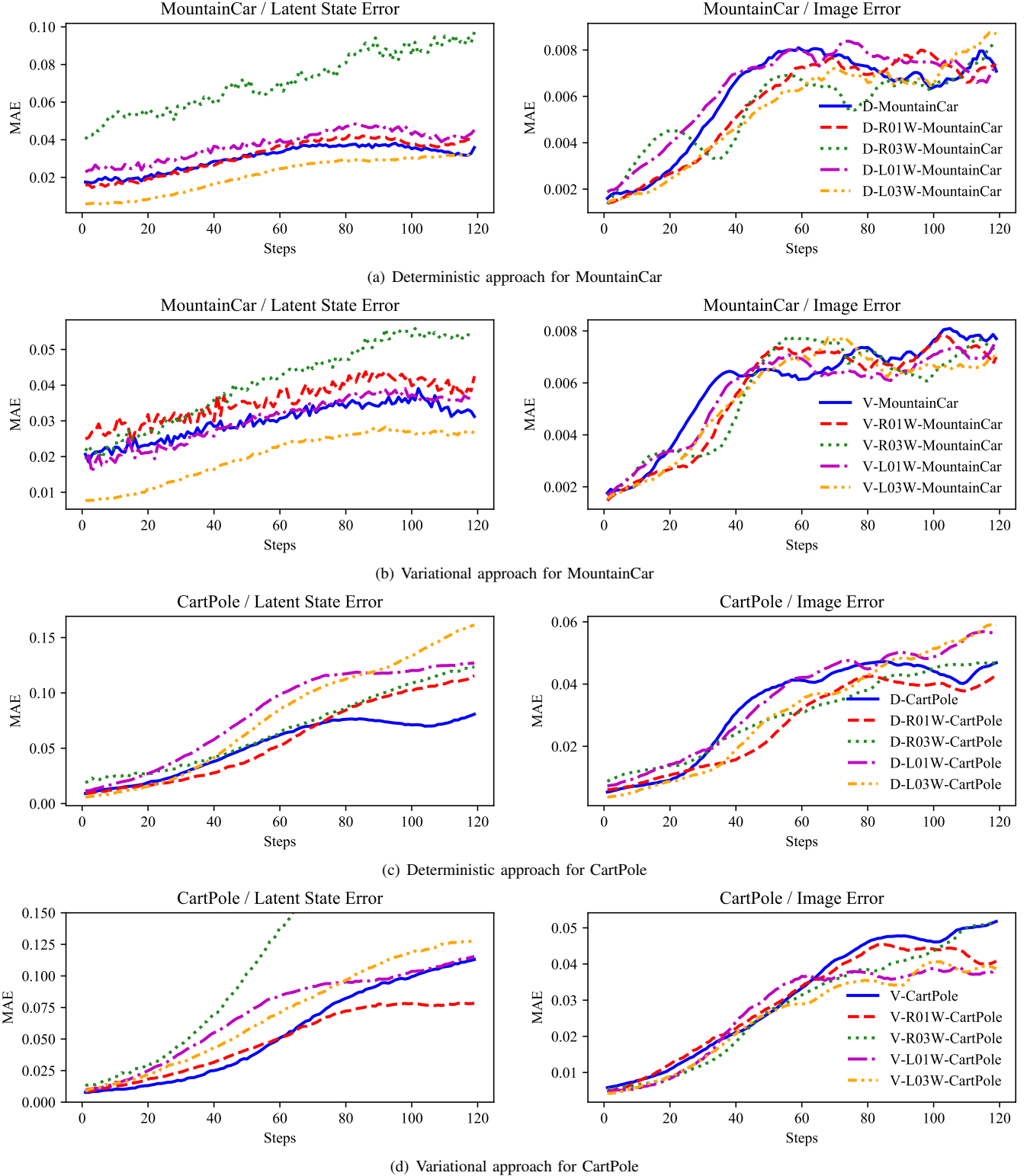


Fig. 5. Prediction MAE with the deterministic and variational approaches for MountainCar and CartPole tasks. The left and right columns subfigures respectively show the MAE of prediction latent states and reconstruction images with different auxiliary weights in (14). Where ‘D’ denotes that CKNet adopts the deterministic approach for the encoder while ‘V’ denotes the variational approach. ‘R0 $\star$ W’ and ‘L0 $\star$ W’ indicate that  $\tau_p$  and  $\tau_l$  in (14) are equal to  $0.01 \times \star$  respectively, otherwise both  $\tau_p$  and  $\tau_l$  are equal to zero. The MAE of each curve are calculated with 30 episodes of prediction.

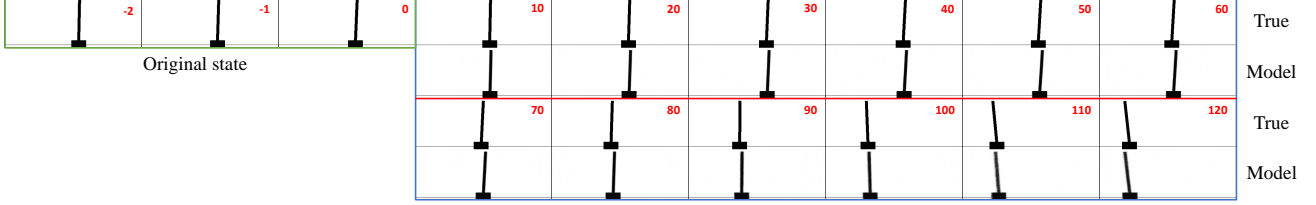


Fig. 6. The prediction of CartPole task. The solid red line divides the picture into two layers and each layer has two rows. The up row denotes the ground truth while the second row denotes the generated images via linear prediction in  $\mathcal{V}$ . Besides, the up left numbers denote the prediction steps.

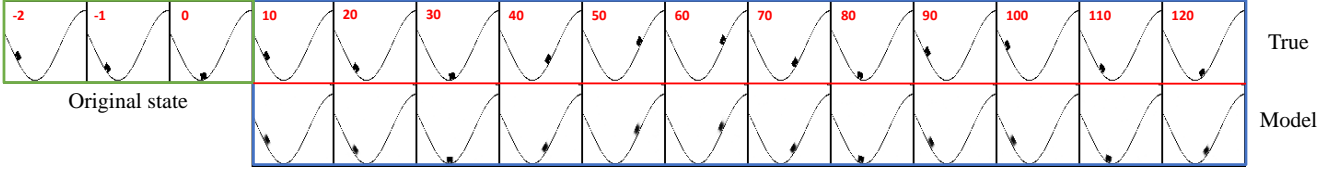


Fig. 7. The prediction of MountainCar task. There are two rows divided via the solid red line. The up row denotes the truth ground while the bottom one denotes generated images by the decoder with predicted states in  $\mathcal{V}$ . The up left number of the first row denotes the corresponding prediction step of each blue frame.

- [10] M. O. Williams, M. S. Hemati, S. T. Dawson, I. G. Kevrekidis, and C. W. Rowley, “Extending data-driven koopman analysis to actuated systems,” *IFAC-PapersOnLine*, vol. 49, no. 18, pp. 704–709, 2016.
- [11] M. Korda and I. Mezić, “Linear predictors for nonlinear dynamical systems: Koopman operator meets model predictive control,” *Automatica*, vol. 93, pp. 149–160, 2018.
- [12] Y. Igarashi, M. Yamakita, J. Ng, and H. H. Asada, “Mpc performances for nonlinear systems using several linearization models,” in *2020 American Control Conference (ACC)*. IEEE, 2020, pp. 2426–2431.
- [13] C. Schütte, P. Koltai, and S. Klus, “On the numerical approximation of the perron-frobenius and koopman operator,” *Journal of Computational Dynamics*, vol. 3, no. 1, pp. 51–79, 2017.
- [14] M. Korda and I. Mezić, “On convergence of extended dynamic mode decomposition to the koopman operator,” *Journal of Nonlinear Science*, 2017.
- [15] J. Morton, F. D. Witherden, A. Jameson, and M. J. Kochenderfer, “Deep dynamical modeling and control of unsteady fluid flows,” *arXiv preprint arXiv:1805.07472*, 2018.
- [16] Z. Ping, Z. Yin, X. Li, Y. Liu, and T. Yang, “Deep koopman model predictive control for enhancing transient stability in power grids,” *International Journal of Robust and Nonlinear Control*, 2020.
- [17] Y. Xiao, X. Zhang, X. Xu, X. Liu, and J. Liu, “A deep learning framework based on koopman operator for data-driven modeling of vehicle dynamics,” *arXiv preprint arXiv:2007.02219*, 2020.
- [18] A. Mardt, L. Pasquali, H. Wu, and F. Noé, “Vampnets for deep learning of molecular kinetics,” *Nature communications*, vol. 9, no. 1, pp. 1–11, 2018.
- [19] T. Xie, A. France-Lanord, Y. Wang, Y. Shao-Horn, and J. C. Grossman, “Graph dynamical networks for unsupervised learning of atomic scale dynamics in materials,” *Nature communications*, vol. 10, no. 1, pp. 1–9, 2019.
- [20] A. Avila and I. Mezić, “Data-driven analysis and forecasting of highway traffic dynamics,” *Nature communications*, vol. 11, no. 1, pp. 1–16, 2020.
- [21] S. L. Brunton, B. W. Brunton, J. L. Proctor, E. Kaiser, and J. N. Kutz, “Chaos as an intermittently forced linear system,” *Nature communications*, vol. 8, no. 1, pp. 1–9, 2017.
- [22] J. Morton, F. D. Witherden, and M. J. Kochenderfer, “Deep variational koopman models: Inferring koopman observations for uncertainty-aware dynamics modeling and control,” in *Twenty-Eighth International Joint Conference on Artificial Intelligence IJCAI-19*, 2019.
- [23] S. E. Otto and C. W. Rowley, “Linearly recurrent autoencoder networks for learning dynamics,” *SIAM Journal on Applied Dynamical Systems*, vol. 18, no. 1, pp. 558–593, 2019.
- [24] B. Lusch, J. N. Kutz, and S. L. Brunton, “Deep learning for universal linear embeddings of nonlinear dynamics,” *Nature communications*, vol. 9, no. 1, pp. 1–10, 2018.
- [25] C. J. Ostafew, A. P. Schoellig, T. D. Barfoot, and J. Collier, “Learning-based nonlinear model predictive control to improve vision-based mobile robot path tracking,” *Journal of Field Robotics*, vol. 33, no. 1, pp. 133–152, 2016.
- [26] V. Mnih, K. Kavukcuoglu, D. Silver, A. A. Rusu, J. Veness, M. G. Bellemare, A. Graves, M. Riedmiller, A. K. Fidjeland, G. Ostrovski et al., “Human-level control through deep reinforcement learning,” *nature*, vol. 518, no. 7540, pp. 529–533, 2015.
- [27] T. Haarnoja, A. Zhou, P. Abbeel, and S. Levine, “Soft actor-critic: Off-policy maximum entropy deep reinforcement learning with a stochastic actor,” in *International Conference on Machine Learning*. PMLR, 2018, pp. 1861–1870.
- [28] J. Schrittwieser, I. Antonoglou, T. Hubert, K. Simonyan, L. Sifre, S. Schmitt, A. Guez, E. Lockhart, D. Hassabis, T. Graepel et al., “Mastering atari, go, chess and shogi by planning with a learned model,” *Nature*, vol. 588, no. 7839, pp. 604–609, 2020.
- [29] M. Laskin, A. Srinivas, and P. Abbeel, “Curl: Contrastive unsupervised representations for reinforcement learning,” in *International Conference on Machine Learning*. PMLR, 2020, pp. 5639–5650.
- [30] D. Hafner, T. Lillicrap, I. Fischer, R. Villegas, D. Ha, H. Lee, and J. Davidson, “Learning latent dynamics for planning from pixels,” in *International Conference on Machine Learning*, 2019, pp. 2555–2565.
- [31] I. U. Haq and Y. Kawahara, “Universal modal embedding of dynamics in videos and its applications,” 2019.
- [32] B. van der Heijden, L. Ferranti, J. Kober, and R. Babuska, “Deepkoco: Efficient latent planning with an invariant koopman representation,” *arXiv preprint arXiv:2011.12690*, 2020.